# REPORT DOCUMENTATION PAGE

*Form Approved*
*OMB No. 0704-0188*



| 1. REPORT DATE *(DD-MM-YYYY)* | 2. REPORT TYPE | 3. DATES COVERED *(From - To)* |
|---|---|---|
| 20-NOV-2003 | Journal article (refereed) | |

**4. TITLE AND SUBTITLE**
Modeling Sheet Flow Sediment Transport In Wave Bottom Boundary Layers Using DEM

5a. CONTRACT NUMBER

5b. GRANT NUMBER

5c. PROGRAM ELEMENT NUMBER

**6. AUTHOR(S)**
Joseph Calantoni K TODD HOLLAND Thomas G. Drake

5d. PROJECT NUMBER

5e. TASK NUMBER

5f. WORK UNIT NUMBER
74-8544-04

**7. PERFORMING ORGANIZATION NAME(S) AND ADDRESS(ES)**
Naval Research Laboratory
Marine Geoscience Division
Stennis Space Center, MS 39529-5004

**8. REPORTING ORGANIZATION REPORT NUMBER**
NRL/JA/7440--03-1014

**9. SPONSORING/MONITORING AGENCY NAME(S) AND ADDRESS(ES)**
Office of Naval Research
800 N. Quincy Street
Arlington, VA 22217

**10. SPONSOR/MONITOR'S ACRONYM(S)**
ONR

**11. SPONSOR/MONITOR'S REPORT NUMBER(S)**

**12. DISTRIBUTION/AVAILABILITY STATEMENT**
Approved for public release,distribution is unlimited

**13. SUPPLEMENTARY NOTES**

20040928 019

**14. ABSTRACT**

Sediment transport in oscillatory boundary layers is a driving mechanism of coastal geomorphologic change. Most formulae for bed load transport in nearshore regions subsume the smallest scale physics of the phenomena by parameterizing interactions between particles. In contrast, we directly simulate granular physics in the wave bottom boundary layer using a discrete element model comprising a three-dimensional particle phase coupled to a one-dimensional fluid phase via Newton's Third Law through forces of buoyancy, drag, and added mass. The particulate sediment phase is modeled using discrete, non-spherical particles formed by overlapping two spheres. Both the size of each sphere and the degree of overlap can be varied for these composite particles to generate a range of non-spherical grains. Simulations of the critical angle for particles having a range of shapes effectively demonstrate the effects of particle shape; the critical angle, ...

**15. SUBJECT TERMS**
sediment, boundary layers, discrete element model

| 16. SECURITY CLASSIFICATION OF: | | | 17. LIMITATION OF ABSTRACT | 18. NUMBER OF PAGES | 19a NAME OF RESPONSIBLE PERSON |
|---|---|---|---|---|---|
| a. REPORT | b. ABSTRACT | c. THIS PAGE | | | Joseph Calantoni |
| Unclassified | Unclassified | Unclassified | Unlimited | 26 | 19b. TELEPHONE NUMBER *(Include area code)* 228-688-4435 |

10.1098/rsta.2004.1427



THE ROYAL SOCIETY

# Modelling sheet-flow sediment transport in wave-bottom boundary layers using discrete-element modelling

BY JOSEPH CALANTONI[1], K. TODD HOLLAND[1] AND THOMAS G. DRAKE[2]

[1]*Naval Research Laboratory, Marine Geosciences Division, Code 7440.3, Building 1005, Stennis Space Center, MS 39529, USA* (joec@nrlssc.navy.mil)

[2]*Office of Naval Research, Coastal Geosciences Program, 321CG, 800 N. Quincy St., Arlington, VA 22217, USA*

Sediment transport in oscillatory boundary layers is a process that drives coastal geomorphological change. Most formulae for bed-load transport in nearshore regions subsume the smallest-scale physics of the phenomena by parametrizing interactions amongst particles. In contrast, we directly simulate granular physics in the wave-bottom boundary layer using a discrete-element model comprised of a three-dimensional particle phase coupled to a one-dimensional fluid phase via Newton's third law through forces of buoyancy, drag and added mass. The particulate sediment phase is modelled using discrete particles formed to approximate natural grains by overlapping two spheres. Both the size of each sphere and the degree of overlap can be varied for these composite particles to generate a range of non-spherical grains. Simulations of particles having a range of shapes showed that the critical angle—the angle at which a grain pile will fail when tilted slowly from rest—increases from approximately 26° for spherical particles to nearly 39° for highly non-spherical composite particles having a dumbbell shape. Simulations of oscillatory sheet flow were conducted using composite particles with an angle of repose of approximately 33° and a Corey shape factor greater than about 0.8, similar to the properties of beach sand. The results from the sheet-flow simulations with composite particles agreed more closely with laboratory measurements than similar simulations conducted using spherical particles. The findings suggest that particle shape may be an important factor for determining bed-load flux, particularly for larger bed slopes.

**Keywords: sediment transport; bed load; wave-bottom boundary layer; discrete-element model; non-spherical particle**

## 1. Introduction

Predicting the morphological evolution of sandy coastlines from the highest uprush of swash offshore to the edge of the surf zone where waves begin to break is a problem

One contribution of 12 to a Theme 'Discrete-element modelling: methods and applications in the environmental sciences'.

with social, economic and scientific significance. Despite the apparent accessibility of the phenomena of interest—namely, the motion of sand under the forcing of waves and currents—the predictive capability of existing models for nearshore evolution is limited to qualitative estimates of bulk behaviours. Given adequate forcing, sediment transport in the nearshore responds in two dominant modes: bed-load transport, in which grains collide, slide, bounce and roll in close proximity to the bed; and suspended load, in which grains are lifted from the bed by fluid turbulence and suspended within the water column. We focus on a special case of bed-load transport called 'sheet flow', which is characterized by high-concentration flows resulting from intense wave/current forcing where the local bed becomes nominally planar and sediment moves in a thin sheet that may be several centimetres thick with a distinct upper surface. When the waves and currents are large we believe sheet flow is a primary agent of bathymetric evolution.

Direct measurements of bed-load transport rates in the surf zone do not exist due to a fundamental lack of technology. The use of sediment traps and bathymetric surveys are two of the best methods available to infer bed-load transport rates. Also, detailed measurements of bulk properties in the sheet layer (e.g. concentration, velocity, fluctuation energy, stress) are nearly impossible to obtain with present technologies.

The relatively simple geometry of sheet-flow transport makes it a well-suited problem for study with a discrete-element model (DEM). Drake & Calantoni (2001) used a DEM to study sheet-flow transport in the surf zone where sediment particles were modelled as spheres. Although the Drake & Calantoni (2001) DEM is a useful tool for studying the general behaviour of sheet flow, recent advances in computing technology now make it possible to simulate non-spherical particle shapes and examine the effect of shape on bed-load transport phenomena. Consider the critical angle, $\phi$, as that at which a pile of grains will experience failure solely under the influence of gravity. The critical angle of beach sand is much larger than that of frictional, spherical particles having the same distribution of sizes as the natural sand. We hypothesize that particle shape significantly influences the static bed strength of non-cohesive sediments, a key determinant of bed-load flux, and test this hypothesis by approximating the shape of sand grains with non-spherical composite particles constructed by joining two partial spheres of different radii (figure 1).

Simulations demonstrated that there exists a composite particle shape where a bed of these particles exhibits a coefficient of static friction similar to beach sand, $\tan\phi \approx 0.63$. The same composite particle was then used to simulate sheet-flow transport conditions based on the laboratory data of King (1991). The sheet-flow simulations showed that the bed-load flux agreed well with the laboratory measurements for gently sloping beds, $|\tan\beta| \leqslant 0.1$. At larger bed slopes and higher transport rates the simulations suggested that particle shape could be an important parameter for predicting bed-load flux.

## 2. DEM for sheet-flow transport

The new DEM described here alters the model of Drake & Calantoni (2001) by allowing the shape of sediment grains to be simulated with non-spherical composite particles. The DEM comprises a three-dimensional Lagrangian particle model coupled to a one-dimensional Eulerian fluid model. The particle and fluid phases are

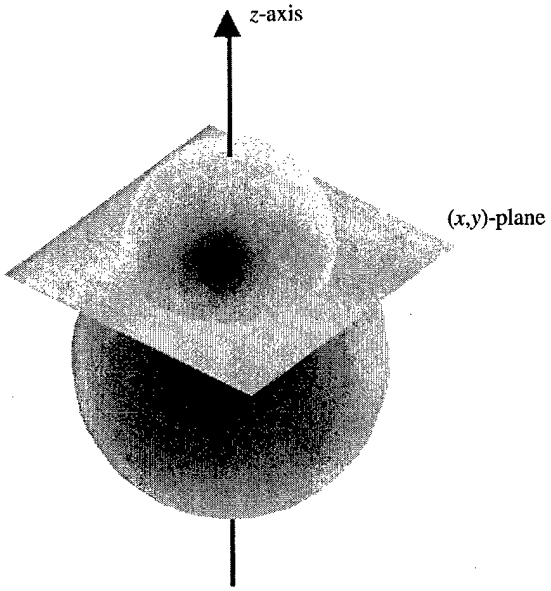


Figure 1. An image of a composite particle is shown where the finite plane represents the plane of separation of the two partial spheres. The initial body coordinate system chosen to solve the inertia tensor problem put the axis of symmetry of the composite particle along the positive $z$-axis. The symmetry of the particle allows for the orientation of the $x$- and $y$-axes to be arbitrarily specified. Here only the location of the $(x, y)$-plane is shown.

coupled at every model time-step via Newton's third law through fluid–particle forces of buoyancy, drag and added mass. An eddy-viscosity-based model determined from a mixing-length-governed vertical momentum transfer between discrete fluid elements completes a self-consistent physical description of the sheet-flow process. The soft sphere interactions between individual particles are modelled exactly as in Drake & Calantoni (2001). However, the shape of simulated sand grains is no longer restricted to be spherical.

### (*a*) *The composite particle*

The motivation for choosing to construct non-spherical particles in this manner was largely guided by the fact that for the composite particle the moments of inertia are solvable analytically in the appropriate coordinate system. Additionally, efficient algorithms for detecting contacts between individual spheres could be used to detect contacts between composite particles. The following subsections provide the necessary analytical solutions and explain how the simulations compute motions for the composite particle.

#### (i) *Volume calculation*

A cylindrical coordinate system with the positive $z$-axis pointing from the centre of sphere 1 to the centre of sphere 2, where $R_1 \geqslant R_2$, was a suitable choice of body coordinates for performing the volume integration of the composite particle

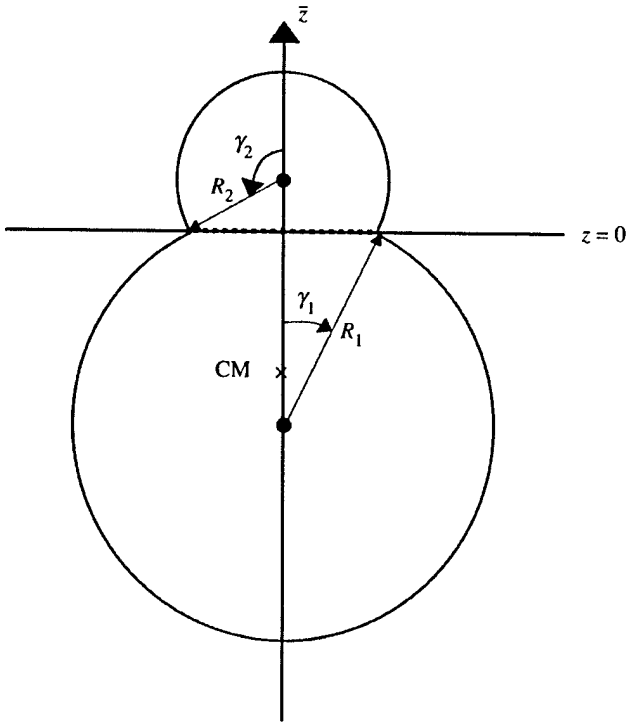


Figure 2. A composite particle in plan view (maximum projected area). The origin for the coordinate system was chosen at the centre of the disc of intersection of the two partial spheres. The symmetry axis of the composite particle is chosen to coincide with the $z$-axis allowing the two partial spheres to be separated by the plane $z = 0$. Partial sphere 1 with radius $R_1$ is placed below the plane of separation, $z = 0$, while partial sphere 2 with radius $R_2$ is placed above the plane of separation with the positive $z$-axis pointing from the centre of partial sphere 1 to the centre of partial sphere 2. The angles $\gamma_1$ and $\gamma_2$ are measured down from the positive $z$-axis about the centre of each respective partial sphere.

(figure 2). The plane $z = 0$ separates the composite particle into two partial spheres allowing the volume integration to be separated into a sum over the two partial spheres, $V = V_1 + V_2$. Using the cylindrical body coordinate system for the composite particle defined in figure 2, where the origin is placed at the centre of the disk of intersection of the two partial spheres, the volume integral becomes

$$V = \int_0^{\sqrt{R_1^2-(z+R_1\cos\gamma_1)^2}} r\,\mathrm{d}r \int_0^{2\pi} \mathrm{d}\theta \int_{-R_1(1+\cos\gamma_1)}^{0} \mathrm{d}z + \int_0^{\sqrt{R_2^2-(z+R_2\cos\gamma_2)^2}} r\,\mathrm{d}r \int_0^{2\pi} \mathrm{d}\theta \int_0^{R_2(1-\cos\gamma_2)} \mathrm{d}z. \quad (2.1)$$

Performing the integration yields

$$V = \tfrac{1}{3}\pi[R_1^3(2 + 3\cos\gamma_1 - \cos^3\gamma_1) + R_2^3(2 - 3\cos\gamma_2 + \cos^3\gamma_2)], \quad (2.2)$$

the volume of the composite particle.

(ii) *Quantifying the shape of natural particles*

Researchers have constructed a variety of methods to describe the shape of a natural clastic sedimentary particle simply with a single parameter in addition to some measure of the particle diameter. Classifying and describing the shape of natural particles has often been motivated by the desire to find a functional relationship between shape and the settling velocity (Dietrich 1982). Our motivation, conversely, was to construct a composite particle that exhibited the same critical angle (or internal angle of static friction) as natural beach sand. The shape of composite particles we constructed was quantified with the Corey shape factor (CSF) (Corey 1949). The CSF is not the only way to quantify the shape of natural particles: the Wadell sphericity (Wadell 1932) and the maximum projection sphericity (MPS) are other popular factors for sediment shape classification (e.g. Middleton & Southard 1984). The physical limits of the composite particle ranged from a sphere to a perfect dumbbell ($R_2/R_1 = 1$, $\gamma_1 = 0$, $\gamma_2 = \pi$). For this range of shapes the CSF assumes values from 0.71 to 1, the Wadell sphericity assumes values from 0.63 to 1, and the MPS assumes values from 0.79 to 1. In the limit where $R_2$ and $\gamma_1$ go to zero the composite particle becomes a sphere and the model presented here is identical to the DEM of Drake & Calantoni (2001). In the following sections we describe simulations to determine a composite particle shape having the same critical angle as beach sand, and a second set of simulations of oscillatory sheet flow using that composite shape for inter-comparison between laboratory experiments.

(iii) *Centre of mass*

The position of the centre of mass (CM) for each composite particle lies on the $z$-axis because of axial symmetry, and the $z$-coordinate of the CM of each partial sphere was found by integrating to obtain (e.g. Marion & Thornton 1988, example 8.1)

$$z_1 = \frac{\pi\rho_1 R_1^4}{M_1}\left(\tfrac{1}{4} + \tfrac{2}{3}\cos\gamma_1 + \tfrac{1}{2}\cos^2\gamma_1 - \tfrac{1}{12}\cos^4\gamma_1\right), \tag{2.3a}$$

$$z_2 = \frac{\pi\rho_2 R_2^4}{M_2}\left(\tfrac{1}{4} - \tfrac{2}{3}\cos\gamma_2 + \tfrac{1}{2}\cos^2\gamma_2 - \tfrac{1}{12}\cos^4\gamma_2\right), \tag{2.3b}$$

where $M_1$ and $M_2$ are the masses of partial sphere 1 and 2, respectively. Now the $z$-coordinate of the CM for the composite particle is given by

$$z_{\mathrm{CM}} = \frac{1}{M_1 + M_2}(M_1 z_1 + M_2 z_2). \tag{2.4}$$

(iv) *Principal moments of inertia*

The inertia tensor for the composite particle is computed using the body coordinate system with the integration limits on the volume defined above. The inertia tensor is calculated considering the density of each partial sphere to be constant and uniform. Performing the integrations (e.g. Goldstein 1980, eqn (5.8)) gives a diagonal inertia tensor of the form

$$I = \begin{pmatrix} I_1 & 0 & 0 \\ 0 & I_2 & 0 \\ 0 & 0 & I_3 \end{pmatrix}, \tag{2.5}$$

where

$$I_1 = I_2 = \frac{\pi\rho_1 R_1^5}{60}[(1+\cos\gamma_1)(16+29\cos\gamma_1+11\cos^2\gamma_1-\cos^3\gamma_1+\cos^4\gamma_1)] + \frac{\pi\rho_2 R_2^5}{60}[(1-\cos\gamma_2)(16-29\cos\gamma_2+11\cos^2\gamma_2+\cos^3\gamma_2+\cos^4\gamma_2)] \tag{2.6a}$$

and

$$I_3 = \frac{\pi\rho_1 R_1^5}{30}[(1+\cos\gamma_1)(8+7\cos\gamma_1-7\cos^2\gamma_1-3\cos^3\gamma_1+3\cos^4\gamma_1)] + \frac{\pi\rho_2 R_2^5}{30}[(1-\cos\gamma_2)(8-7\cos\gamma_2-7\cos^2\gamma_2+3\cos^3\gamma_2+3\cos^4\gamma_2)]. \tag{2.6b}$$

(v) *Principal moments of inertia about the CM*

The principal moments of inertia about the CM are required to solve Euler's equations for the rotational motion of a rigid body. In general, the CM of a composite particle does not coincide with the origin of the body coordinate system. Applying the parallel axis theorem, the principal moments of inertia about the CM of the composite particle shown in figure 2 become

$$I_1' = I_1 - (M_1+M_2)z_{\mathrm{CM}}^2, \tag{2.7a}$$

$$I_2' = I_2 - (M_1+M_2)z_{\mathrm{CM}}^2, \tag{2.7b}$$

$$I_3' = I_3. \tag{2.7c}$$

(vi) *Contact detection and contact forces*

Use of spheres to construct composite particles allows use of highly optimized routines to detect contacts between spheres. The contact detection algorithm employed in this model is based on the method of Munjiza & Andrews (1998). The normal and tangential forces generated at the contact points between partial sphere pairs are calculated using the same interaction models as Drake & Calantoni (2001). Forces are then re-expressed in terms of the normal and tangential components relative to the CM of the respective composite particle. For each individual force determined to be tangential to the CM of a composite particle, a moment arm is constructed and the torque is calculated. The sum of the torque on each composite particle is then calculated along with the sum of the force through the CM.

(vii) *Fluid–fluid interactions*

The fluid phase of the model used the same interactions as Drake & Calantoni (2001). A one-dimensional eddy-viscosity model determined from a mixing length was driven by a time-varying horizontal pressure gradient with sinusoidal forcing,

$$F \propto \cos(\omega t), \tag{2.8}$$

where $\omega$ is the angular frequency. The applied horizontal pressure gradient was constant across the entire domain and acted on both the fluid and the particles embedded in the wave-bottom boundary layer (WBBL). Computationally, the fluid model was implemented with a stack of discrete fluid slabs, such that if the CM of a particle was located within a slab, then all fluid–particle interactions occurred with that slab. Likewise, the total volume of the particles located in a fluid slab appropriately reduced the volume of fluid contained in the slab.

(viii) *Fluid–particle interactions*

Fluid–particle forces are determined by considering the forces on a spherical particle with the equivalent mass. The governing equation for translational motion of a composite particle is given by (e.g. Madsen 1991)

$$\rho_{\mathrm{s}} V_{\mathrm{s}} \frac{\mathrm{d}\boldsymbol{u}_{\mathrm{s}}}{\mathrm{d}t} = (\rho_{\mathrm{s}} - \rho) V_{\mathrm{s}} \boldsymbol{g} + \rho V_{\mathrm{s}} \left.\frac{\mathrm{D}\boldsymbol{u}}{\mathrm{D}t}\right|_{z=\infty} + \rho V_{\mathrm{s}} c_{\mathrm{m}} \left( \frac{\mathrm{D}\boldsymbol{u}}{\mathrm{D}t} - \frac{\mathrm{d}\boldsymbol{u}_{\mathrm{s}}}{\mathrm{d}t} \right) + \tfrac{1}{2} \rho C_{\mathrm{D}}^{*} A |\boldsymbol{u} - \boldsymbol{u}_{\mathrm{s}}| (\boldsymbol{u} - \boldsymbol{u}_{\mathrm{s}}) + \boldsymbol{F}_{\Phi}, \quad (2.9)$$

where $\rho_{\mathrm{s}}$ and $\rho$ are the particle and fluid densities, respectively, $V_{\mathrm{s}}$ is the particle volume, $\boldsymbol{g}$ is the acceleration due to gravity, $\boldsymbol{u}_{\mathrm{s}}$ and $\boldsymbol{u}$ are the particle and fluid velocities, respectively, and $A$ is the projected area of the equivalent spherical particle. All derivatives are evaluated at the CM of the particle unless specifically noted. The first term on the right-hand side represents the particle buoyancy, the second term is the horizontal pressure gradient acting on the particle, and the third term represents the added-mass effect with the coefficient of added mass $c_{\mathrm{m}} = 0.5$ (Batchelor 1967). The fourth term represents the particle drag force with the drag coefficient $C_{\mathrm{D}}^{*}$, given by an approximate fit to the empirical drag law for spheres, including a correction $c^{*}$, based on local particle concentration (e.g. Richardson & Zaki 1954),

$$C_{\mathrm{D}}^{*} = c^{*}(24 Re_{\mathrm{s}}^{-1} + 4 Re_{\mathrm{s}}^{-1/2} + 0.4), \quad (2.10)$$

where

$$c^{*} = (1 - c - \tfrac{1}{3}c^{2})^{-5/2}, \quad (2.11)$$

$Re_{\mathrm{s}}$ is the relative particle Reynolds number, and $c$ is the local particle concentration. Fluid–particle forces resulting from the rotation of particles are ignored along with lift forces. The final term in equation (2.9), $\boldsymbol{F}_{\Phi}$, represents the sum of interparticle forces acting through the CM of the particle.

### (*b*) *Simulations with composite particles*

(i) *Critical-angle simulations*

A suite of simulations was performed using composite particles that nearly span the allowable range of the CSF. The critical angle, $\phi$, was measured for eight different beds of 250 identical composite particles, formed by fixing the value of the ratio of $R_2/R_1$ and then allowing the value of $\gamma_2$ (defined in figure 2) to vary from 0 to $\pi$ in increments of $\pi/8$. Here the critical angle was taken to be the angle at which a pile of grains fails under the force of gravity, which is also referred to as the internal angle of static friction. For the case of $\gamma_2 = 0$, the composite particle reduces

to a sphere with radius given by $R_1$. Values of $R_1 = 2.5$ mm and $R_2 = 1.25$ mm were chosen so that $R_2/R_1 = \frac{1}{2}$. Simulations were performed for particles under the influence of gravity in a vacuum; no interstitial fluid was modelled in the critical-angle simulations. Simulations began by settling the particles from a regular lattice onto a smooth basal plane having a row of fixed spheres attached at one end to prevent the wholesale sliding of the granular assemblage. Periodic boundary conditions were used in the two lateral directions. The bed was then 'tilted' by rotating the gravity force vector in discrete increments at a rate of $0.1° \text{ s}^{-1}$. Once failure occurred, the gravity vector was rotated back in the same manner until it was again orthogonal to the bed. Ancillary tests showed that simulating one second of real time after changing the direction of the gravity vector was sufficient to measure the critical angle with a precision of 0.1°.

(ii) *Sheet-flow simulations of King's experiments*

The experiments of King (1991) served as a useful benchmark to validate the model presented here for sheet-flow transport of coarse sediments under waves. King's oscillatory flow tunnel experiments using a distribution of quartz sediment with a mean diameter of 1.1 mm provide sediment transport rates for half-cycle oscillatory flows in a number of horizontal and tilted-bed configurations. The sheet-flow simulations were performed with the composite particle shape that demonstrated a critical angle similar to beach sand, $\phi \approx 33°$ (Bagnold 1956). Sheet-flow simulations with spheres were also performed and were shown to emphasize the significant effect of particle shape on bulk sediment transport rates predicted by the model. The set of experiments simulated here use a half-period sine wave with a period $T = 4.64$ s, and a maximum velocity amplitude of $1.18 \text{ m s}^{-1}$, over a range of bed slopes, $-0.096 \leqslant \tan\beta \leqslant 0.16$, where $\beta$ is the angle of inclination of the bed in the direction of flow.

The simulations used 1600 particles where every composite particle had the same shape with a distribution of sizes similar to the distribution used in the King (1991) experiments. The mass of each of the 1600 unique composite particles was held constant as the shape was changed to a sphere, ensuring that the only difference in the sheet-flow simulations with spheres and composite particles was the particle shape. The density of particles in all simulations was constant and equivalent to the density of quartz sediment, $\rho_s = 2650 \text{ kg m}^{-3}$. For these sheet-flow simulations, the physical dimensions of the computational domain were approximately 2 cm along the flow direction, 1 cm transverse to the flow, and 4 cm in the vertical. A stack of 40 fluid slabs, each 1 mm thick, was used to model the fluid.

## 3. Simulation results

### (a) *Critical-angle simulations*

The simulations performed demonstrated that there exists a composite particle shape that does exhibit a critical angle similar to beach sand. The critical angle, $\phi$, is plotted as a function of the CSF in figure 3. Each point is the average value of 10 simulations with one standard deviation plotted above and below. A bed of identical composite particles with the ratio $R_2/R_1 = \frac{1}{2}$ and $\gamma_2 = 5\pi/8$ having CSF = 0.84 exhibited an average critical angle of 32.9°. Naturally occurring sediments have an upper mean

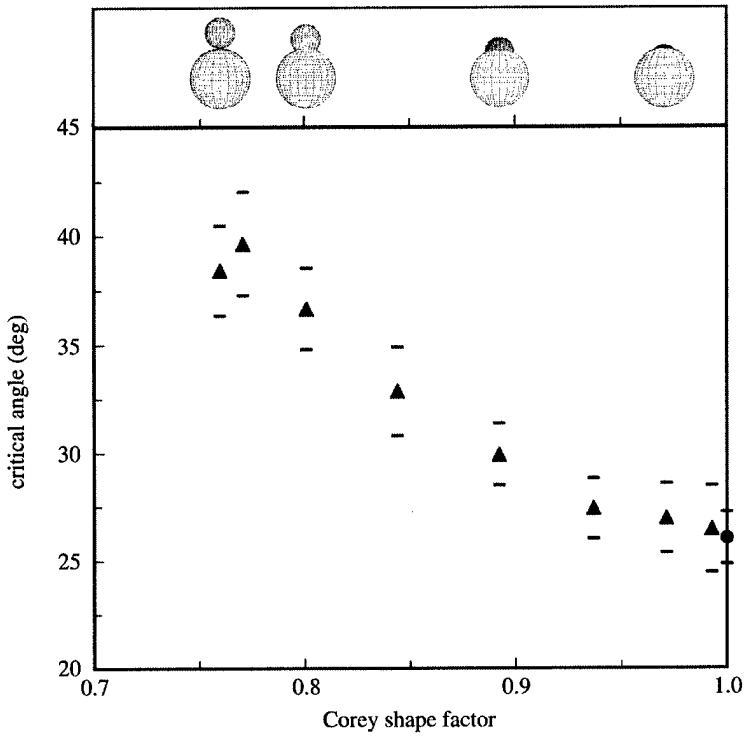


Figure 3. Each triangle is the average critical angle of 10 successive simulations with one standard deviation plotted above and below each point for the ratio $R_2/R_1 = \frac{1}{2}$, with the value of $\gamma_2$ increasing smoothly from 0 to $\pi$, in increments of $\pi/8$, as the CSF decreases from 1 to 0.76. Shown in the upper panel are images of composite particles located in the position of their corresponding CSF value with $\gamma_2 = \pi$, $3\pi/4$, $\pi/4$ and $\pi/8$ from left to right. The circle represents the critical angle for a bed of identical spheres, CSF = 1. The composite particle with the ratio, $R_2/R_1 = \frac{1}{2}$, $\gamma_2 = 5\pi/8$, having CSF = 0.84, exhibited an average critical angle of 32.9°, suggesting that for the range of shapes simulated this composite particle possesses properties very similar to beach sand.

CSF value of about 0.8 (Dietrich 1982), suggesting that we found a composite particle that simultaneously satisfied shape and critical-angle characteristics of beach sand.

Simulations of a bed of 250 identical spheres with radius $R = 2.5$ mm were performed in exactly the same manner as the composite particles, and the critical-angle value was found to be 26° (figure 3), in good agreement with experiments performed on rough glass beads in rotating drums (Jaeger *et al.* 1989).

### (*b*) *Sheet-flow simulations*

Both spherical and composite particles were used in simulations of sheet-flow transport to allow direct comparisons with the laboratory data of King (1991). Figure 4 depicts net bed-load transport rates from simulations with composite particles and spherical particles along with King's experimental data. Each point in the plot represents the average of at least four trials in both the simulations and experiments. For the simulations, five consecutive wave periods were run with the data from the first

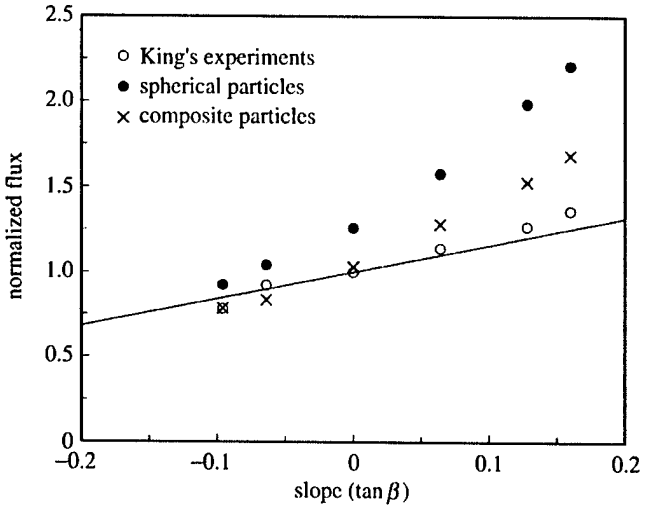


Figure 4. The normalized flux is plotted against the local bed slope for simulations with spheres (•), simulations with composite particles (×), and experimental data (o). All points represent the average flux from at least four half-wave cycles of a sine wave with a period, $T = 4.64$ s, and maximum velocity amplitude of 1.18 m s$^{-1}$. All points are normalized by the flux value from the laboratory measurements over a horizontal bed. The range of values for each point typically does not exceed the size of the symbol shown. The thin line represents the dependence of energetics formulae for bed-load transport on the bed slope, $\tan\beta$. The thin line is scaled to have a value of 1 for a horizontal bed in order to isolate the dependence of the transport formulae on bed slope.

wave period discarded due to transient start-up effects. The range of transport rates for the last four wave periods did not exceed the size of the symbol shown. Likewise, for the experimental data the range of transport rates only slightly exceeded the size of the symbol shown for two of the points.

The time-averaged transport rates from simulations with composite particles were in good agreement with the experimental data. Simulations using composite particles showed improved skill in predicting transport rates over simulations using spheres; in all cases the composite particle simulations showed lower net transport rates for the range of conditions simulated. For the horizontal bed case, the average bed-load flux in the composite particle simulations was within 3% of the average value given by the experiments, whereas the spherical particle simulations were approximately 25% greater than the experimental value. For the highest transport rates the composite particle simulations over-predicted the flux from the experiments by less than 25% compared with 60% over-prediction for the spherical simulations.

Although the experimental data of King (1991) only provide bulk transport rates, the simulations allow detailed examination of sheet-flow phenomena. The average time-series of the flux from the four half-wave cycles over a horizontal bed for both spheres and composite particles is shown in figure 5. The time-series indicate that the times of initiation and cessation of motion are only slightly affected by changing the particle shape. However, the peak flux for the composite particle simulations is approximately 15% less than the peak flux for the spherical simulations. Integrated

over the entire half-wave cycle the net flux for the composite particle simulations is approximately 20% less than the net flux from the spherical simulations.

The sheet-flow simulation results were not sensitive to the particular composite particle shape. We performed an analogous suite of simulations with the ratio $R_2/R_1 = \frac{2}{3}$, and a single shape was found to exhibit a critical angle similar to beach sand by systematically varying the value of $\gamma_2$. When used in the sheet-flow simulations, nearly identical results were obtained to those outlined above, suggesting that the simulation results are robust over a range of composite particles with shape factors similar to beach sand.

## 4. Discussion

The results from DEM simulations show how particle shape directly influences the angle at which a pile of grains will fail, along with bulk bed-load transport rates. The simulations were conducted over a range of conditions involving different particle shapes and various bed slopes. A strong dependency between the grain shape and bed-load flux was observed. The DEM will allow future work to include more simulations to elucidate the role of grain shape, particularly the degree of angularity, in bed-load transport.

The initial simulations (figure 3) demonstrated that as the particle shape was changed from a sphere to a dumbbell the critical angle increased significantly. In particular, the composite particles with $R_2/R_1 = \frac{1}{2}$ and $\gamma_2 = 5\pi/8$ have a critical angle of approximately 33° with CSF = 0.84. These values are characteristic of typical beach sand; this shape was thus used in all sheet-flow simulations. The sheet-flow simulations using composite particles showed greater skill in predicting the bulk bed-load transport rates measured by King (1991) than simulations using spherical particles (figure 4). At small bed slopes and for lower transport rates the simulations using composite particles describe the relevant physics of the laboratory experiments using beach sand well. At larger bed slopes and for higher transport rates the simulations using composite particles showed better accuracy than spheres but did not closely match the experimental data.

One possible reason for the improved accuracy of the composite particles over spheres is the additional inter-granular contacts that occur within a bed of composite particles. For instance, any two ellipsoids can share only one contact point, whereas the composite particles used in our sheet-flow simulations may share up to four contact points between two adjacent composite particles. In this sense, composite particles offer a better approximation to the shape of a sand grain than other regular shapes such as ellipsoids. A bed of composite particles allow a greater resistance to motion that should reduce bed creep along with the number of particles likely to participate in bed-load transport.

An alternative explanation is that composite particles have greater rotational inertia than spheres with the same mass. The only difference between simulations was the particle shape, with the driving force and governing equations for translational motion identical between the two sets of simulations. The peak flux (figure 5) is reduced by nearly 15% in the time-series for the composite particles compared with the time-series for the spherical particles. The observed reduction in peak flux in time-series for the composite particles over spheres (figure 5) indicates that the composite particles dissipate more translational kinetic energy than the spherical particles.

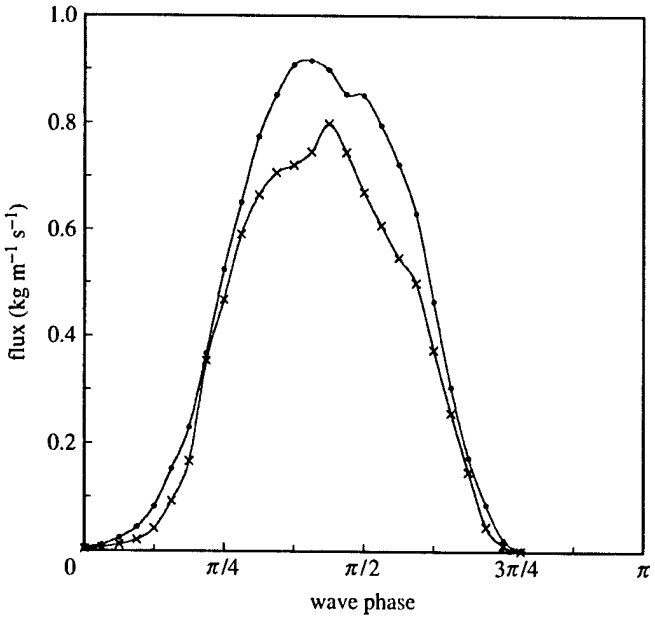


Figure 5. The average time-series of the bed-load flux from four successive half-wave cycles in simulations for spheres (•) and for composite particles (×), where $R_2/R_1 = \frac{1}{2}$, $\gamma_2 = 5\pi/8$. There were no time-series of flux measurements from the experimental data to be used for comparison here. The composite particle time-series showed deviations with initiation and cessation of motion from the spherical time-series. The difference in peak flux between the two time-series illustrated a bulk property of the granular flow that the composite particles exhibited a larger coefficient of kinetic friction than the spherical particles.

At greater slopes, the simulations with both spheres and composite particles do show significant deviations from the laboratory measurements (figure 4). The bed-load flux from simulations with spheres is only in agreement with the laboratory measurements for the smallest transport rates. The bed-load flux from the composite particle simulations remains in agreement with the King experiments for the range of bed slopes $|\tan\beta| \leqslant 0.1$, but over-predicts flux for the largest transport rates. Perhaps the trend could be explained by considering the roundness of the particles. King (1991) reports that the roundness of the quartz sediments used in the experiments were sub-angular to angular, as defined by Shepard & Young (1961). Using the same classification our spherical particles were classified as well rounded, while our composite particles were classified as rounded. Composite particles have greater rotational inertia than spherical particles with the same mass. Likewise, angular grains have greater rotational inertia than composite particles with the same mass. The rotational inertia of individual particles as their shape goes from having three axes of symmetry (spheres) to one axis of symmetry (composite particles) to no symmetry axes (angular grains) will increase bulk-energy dissipation with increasing energy and should result in lower bed-load flux for the most angular sediment grains. The results of the simulations suggest that particle shape is an important parameter for predicting bed-load flux.

### (*a*) *Sediment shape dependence in bed-load transport formulae*

Energetics models (Bowen 1980; Bailard & Inman 1981) describing bed-load transport in the surf zone based on Bagnold's (1966) description of bed-load transport in unidirectional flows contain only one parameter, $\tan(\phi)$, that depends on the shape of the sediment particles, where $\phi$ is the internal angle of static friction of the sediment. We have shown that a composite particle can be constructed to exhibit a value of $\phi$ similar to beach sand. Now, we can examine more closely the particle shape dependence in energetics models for bed-load transport. For the simulated conditions of a unidirectional half-period sine wave the bed-load formula of Bailard & Inman (1981) depends on $\tan\phi$ as follows:

$$q \propto \frac{1}{\tan\phi}\left(1 + \frac{\tan\beta}{\tan\phi}\right), \tag{4.1}$$

where $q$ is the bed-load transport rate and $\tan\beta$ represents the local bed slope along the flow direction.

For flow over a horizontal bed, $\tan\beta = 0$, the bed-load transport rate is inversely proportional to the coefficient of static friction, $\tan\phi$. The time-averaged bed-load flux over a horizontal bed for simulations with composite particles is in excellent agreement with the experimental data for the single point shown in figure 4. The simulations with spheres gave an increase in bed-load flux of approximately 25% over the King experiments for the case of the horizontal bed. The value of $\tan\phi$ for the spheres in simulations was found to be about 0.5. The value of $q$ in equation (4.1) is approximately 25% greater when $\tan\phi = 0.5$ than when $\tan\phi = 0.63$, with $\tan\beta = 0$, suggesting that for bed-load transport over a horizontal bed, the shape parametrization provided by energetics models is consistent with both spherical and composite particle simulations.

For sloping beds, the bed-load transport rate given by equation (4.1) is a linear function of the local bed slope, $\tan\beta$. The thin line shown in figure 4 represents the dependence of bed-load transport on local bed slope given by equation (4.1) with $\tan\phi = 0.63$ (Bagnold 1956). Since King (1991) did not report the value of $\tan\phi$ for the grains used in his laboratory experiments, the vertical offset of the line was adjusted so that the flux value for a horizontal bed goes through the value of the flux from the laboratory data. The laboratory data are in good agreement with the energetics dependence for the entire range of bed slopes shown, given the choice of $\tan\phi$. The composite particle simulations are also in good agreement for the range of bed slopes $-0.1 < \tan\beta < 0.1$. Typically, it is not common to find bed slopes in the surf zone much greater than about 0.1 except on the slip faces of bed forms, suggesting that our composite particle model captured the essential physics for particle shape and local bed slope parametrized by energetics models in equation (4.1). Our expectation is that for higher slopes where flux values can be large, particle shape will have a substantial influence on bed-load flux mechanics, necessitating a modification to the formula given in equation (4.1).

## 5. Conclusions

We have presented a new DEM for sheet-flow transport of coarse sediments in a WBBL under oscillatory flow. The DEM used composite particles to simulate the

non-spherical shape of beach sand. Simulations performed to measure the internal angle of static friction for beds of composite particles reveal that there exists a composite particle that exhibits a similar coefficient of static friction to beach sand, $\tan\phi \approx 0.63$. Additionally, this composite particle has a CSF slightly greater than about 0.8, in the upper range for CSF values of naturally occurring sediments. This composite particle shape that most closely matches the properties of beach sand was then used to simulate sheet-flow transport conditions observed in the laboratory data of King (1991). The simulation results showed that the bed-load flux for gently sloping beds, $|\tan\beta| \leqslant 0.1$, with sinusoidal wave forcing, agrees well with the laboratory measurements. However, the simulations suggested that particle roundness could be an important parameter for predicting bed-load flux at larger bed slopes and higher transport rates.

The simulation results suggest that the composite particle approximation to the shape of a sand grain is useful and robust for discrete-element modelling of bed-load transport phenomena. Comparisons of simulations with both spheres and composite particles with laboratory data indicate that particle shape is an important variable for understanding the bulk properties of sheet flow.

J.C. thanks P. K. Haff for valuable discussion motivating this research. We thank C. S. Thaxton for a review of the analytical solution provided in the paper. This work was performed while J.C. held a National Research Council Research Associateship Award at the Naval Research Laboratory. Research was supported by the Office of Naval Research.

## References

Bagnold, R. A. 1956 The flow of cohesionless grains in fluids. *Phil. Trans. R. Soc. Lond.* A **249**, 235–297.

Bagnold, R. A. 1966 An approach to the sediment transport problem from general physics. US Geological Survey, professional paper 422 (I), pp. 1–37.

Bailard, J. A. & Inman, D. L. 1981 An energetics bedload model for a plane sloping beach—local transport. *J. Geophys. Res. Oceans* **86**(3), 2035–2043.

Batchelor, G. K. 1967 *An introduction to fluid dynamics.* Cambridge University Press.

Bowen, A. J. 1980 Simple models of nearshore sedimentation; beach profiles and longshore bars. In *The coastline of Canada* (ed. S. B. McCann), pp. 1–11. Geological Survey of Canada, paper 80-10.

Corey, A. T. 1949 Influence of shape on the fall velocity of sand grains. MS thesis, Colorado A&M College, Fort Collins, CO, USA.

Dietrich, W. E. 1982 Settling velocity of natural particles. *Water Resources Res.* **18**(6), 1615–1626.

Drake, T. G. & Calantoni, J. 2001 Discrete particle model for sheet flow sediment transport in the nearshore. *J. Geophys. Res. Oceans* **106**(9), 19 859–19 868.

Goldstein, H. 1980 *Classical mechanics*, 2nd edn. Addison-Wesley.

Jaeger, H. M., Liu, C. H. & Nagel, S. R. 1989 Relaxation at the angle of repose. *Phys. Rev. Lett.* **62**(1), 40–43.

King, D. B. 1991 Studies in oscillatory flow bedload sediment transport. PhD thesis, University of California, San Diego, CA, USA.

Madsen, O. S. 1991 Mechanics of cohesionless sediment transport in coastal waters. In *Proc. Specialty Conf. on Quantitative Approaches to Coastal Sediment Processes, 1991* (ed. N. C. Kraus, K. J. Gingerich & D. L. Kriebel), pp. 15–27. New York: ASCE.

Marion, J. B. & Thornton, S. T. 1988 *Classical dynamics of particles and systems*, 3rd edn. Orlando, FL: Harcourt Brace.

Middleton, G. V. & Southard, J. B. 1984 *Mechanics of sediment movement.* Tulsa, OK: SEPM.

Munjiza, A. & Andrews, K. R. F. 1998 NBS contact detection algorithm for bodies of similar size. *Int. J. Numer. Meth. Engng* **43**, 131–149.

Richardson, J. F. & Zaki, W. N. 1954 Sedimentation and fluidisation. *Trans. IChE* **32**, 35–53.

Shepard, F. P. & Young, R. 1961 Distinguishing between beach and dune sands. *J. Sediment. Petrol.* **31**(2), 196–214.

Wadell, H. 1932 Volume, shape, and roundness of rock-particles. *J. Geol.* **40**, 443–451.